Polarization sensitive terahertz imaging: detection of birefringence and optical axis

Stefan Katletz,[1,*] Michael Pfleger,[1] Harald Pühringer,[1] Martin Mikulics,[2] Nico Vieweg,[3] Ole Peters,[3] Benedikt Scherger,[3] Maik Scheller,[3] Martin Koch,[3] and Karin Wiesauer[1]

[1]*Recendt GmbH, Science Park 2, Altenberger Str. 69, 4040 Linz, Austria*
[2]*Peter Grünberg Institute (PGI-9), Forschungszentrum Jülich, 52425 Jülich, Germany*
[3]*Fachbereich Physik, Philipps Universität Marburg, Renthof 5, 35032 Marburg, Germany*
[*]*stefan.katletz@recendt.at*

http://www.recendt.at

Abstract: We present a practicable way to take advantage of the spectral information contained in a broadband terahertz pulse for the determination of birefringence and orientation of the optical axis in a glass fiber reinforced polymer with a single measurement. Our setup employs circularly polarized terahertz waves and a polarization-sensitive detector to measure both components of the electromagnetic field simultaneously. The anisotropic optical parameters are obtained from an analysis of the phase and frequency resolved components of the terahertz field. This method shows a high tolerance against the skew of the detection axes and is also independent of a reference measurement.

OCIS codes: (110.6795) Terahertz imaging; (120.4290) Nondestructive testing; (120.5050) Phase measurement; (230.5440) Polarization-selective devices; (260.1440) Birefringence.

References and links

1. S. Katletz, M. Pfleger, H. Pühringer, N. Vieweg, B. Scherger, B. Heinen, M. Koch, and K. Wiesauer, "Efficient terahertz en-face imaging," Opt. Express **19**, 23042–23053 (2011).
2. M. Born, E. Wolf, and A. Bhatia, *Principles of Optics: Electromagnetic Theory of Propagation, Interference and Diffraction of Light* (Cambridge University Press, 7th ed, 1999).
3. Y.-S. Jin, G.-J. Kim, and S.-G. Jeon, "Terahertz dielectric properties of polymers," J. Korean Phys. Soc. **49**, 513–517 (2006).
4. M. Reid and R. Fedosejevs, "Terahertz birefringence and attenuation properties of wood and paper," Appl. Optics **45**, 2766–2772 (2006).
5. L. Öhrström, A. Bitzer, M. Walther, and F. J. Rühli, "Technical note: terahertz imaging of ancient mummies and bone," Am. J. Phys. Anthropol. **142**, 497–500 (2010).
6. C. Jördens, M. Scheller, S. Wietzke, D. Romeike, C. Jansen, T. Zentgraf, K. Wiesauer, V. Reisecker, and M. Koch, "Terahertz spectroscopy to study the orientation of glass fibres in reinforced plastics," Compos. Sci. Technol. **70**, 472–477 (2010).
7. X. Wang, Y. Cui, W. Sun, J. Ye, and Y. Zhang, "Terahertz polarization real-time imaging based on balanced electro-optic detection," J. Opt. Soc. Am. A **27**, 2387–2393 (2010).
8. T. Hofmann, C. Herzinger, J. L. Tedesco, D. Gaskill, J. Woollam, and M. Schubert, "Terahertz ellipsometry and terahertz optical-hall effect," Thin Solid Films **519**, 2593–2600 (2011).
9. T. Hofmann, D. Schmidt, A. Boosalis, P. Kühne, R. Skomski, C. M. Herzinger, J. A. Woollam, M. Schubert, and E. Schubert, "THz dielectric anisotropy of metal slanted columnar thin films," Appl. Phys. Lett. **99**, 081903–1–3 (2011).

#172500 - $15.00 USD Received 12 Jul 2012; revised 12 Sep 2012; accepted 13 Sep 2012; published 24 Sep 2012

10. D. Grischkowsky, S. Keiding, M. van Exter, and C. Fattinger, "Far-infrared time-domain spectroscopy with terahertz beams of dielectrics and semiconductors," J. Opt. Soc. Am. B **7**, 2006–2015 (1990).
11. E. Castro-Camus, "Polarization-resolved terahertz time-domain spectroscopy," J. Infrared Milli. Terahz. Waves **33**, 418–430 (2012).
12. E. Castro-Camus and M. B. Johnston, "Extraction of the anisotropic dielectric properties of materials from polarization-resolved terahertz time-domain spectra," J. Opt. A-Pure Appl. Op. **11**, 105206–1–6 (2009).
13. E. Castro-Camus, J. Lloyd-Hughes, M. B. Johnston, M. D. Fraser, H. H. Tan, and C. Jagadish, "Polarization-sensitive terahertz detection by multicontact photoconductive receivers," Appl. Phys. Lett. **86**, 254102–1–3 (2005).
14. H. Makabe, Y. Hirota, M. Tani, and M. Hangyo, "Polarization state measurement of terahertz electromagnetic radiation by three-contact photoconductive antenna," Opt. Express **15**, 11650–11657 (2007).
15. N. C. J. van der Valk, W. A. M. van der Marel, and P. C. M. Planken, "Terahertz polarization imaging," Opt. Lett. **30**, 2802–2804 (2005).
16. K. Wiesauer, M. Pircher, E. Götzinger, C. K. Hitzenberger, R. Engelke, G. Ahrens, G. Grützner, and D. Stifter, "Transversal ultrahigh-resolution polarization sensitive optical coherence tomography for strain mapping in materials," Opt. Express **14**, 5945–5953 (2006).
17. A. Redo-Sanchez, N. Karpowicz, J. Xu, and X.-C. Zhang, "Damage and defect inspection with terahertz waves," in "The 4th International Workshop on Ultrasonic and Advanced Methods for Nondestructive Testing and Material Characterization, June 19," (www.ndt.net, 2006), pp. 67–78.
18. S. Ebara, Y. Hirota, M. Tani, and M. Hangyo, "Highly sensitive birefringence measurement in THz frequency region and its application to stress measurement," in "32nd International Conference on Infrared and Millimeter Waves, IRMMW-THz 2007," (2007), pp. 666–667.
19. C. Jördens, M. Scheller, M. Wichmann, M. Mikulics, K. Wiesauer, and M. Koch, "Terahertz birefringence for orientation analysis," Appl. Optics **48**, 2037–2044 (2009).
20. Y. Hirota, R. Hattori, M. Tani, and M. Hangyo, "Polarization modulation of terahertz electromagnetic radiation by four-contact photoconductive antenna," Opt. Express **14**, 4486–4493 (2006).
21. S. Katletz, M. Pfleger, H. Pühringer, N. Vieweg, B. Scherger, B. Heinen, M. Koch, and K. Wiesauer, "Polarization sensitive imaging with pulsed thz radiation," in "International THz Conference," vol. 287 of *Österreichische Computer Gesellschaft*, R. Leitner and T. Arnolds, eds. (2011), pp. 63–67.
22. M. Pfleger, S. Katletz, H. Pühringer, N. Vieweg, B. Scherger, B. Heinen, M. Scheller, M. Mikulics, M. Koch, and K. Wiesauer, "Comparison of polarization-sensitive detection methods of thz radiation," in "International THz Conference," vol. 287 of *Österreichische Computer Gesellschaft*, R. Leitner and T. Arnolds, eds. (2011), pp. 149–154.

1. Introduction

We have effectively converted our scanning Terahertz (THz) imaging setup [1] into a circular polariscope, which detects the phase difference introduced by a slow and fast optical axis but is independent of their orientation [2]. Therefore we are able to determine the birefringence and the orientation of the optical axis by using a polarization sensitive (PS) detector and analyzing the wavelength dependence of the phase difference between horizontal and vertical components of the electromagnetic THz field. Since a single scan of the sample contains enough information for our extraction algorithm, we have combined PS THz imaging with photoelasticity and demonstrate the capability of our setup for a glass fiber reinforced plastic (GFP), which is opaque in the visible. Consequently, THz technology can be more easily applied for orientation analysis in anisotropic materials and stress measurements in polymers, but is not restricted to transparent materials only.

THz radiation features a large penetration depth in many dielectric materials [3, 4] and hence allows for non-destructive measurements even on thick samples [5], which are otherwise opaque in the visible and near-infrared. Anisotropy in a material can arise by, e.g., an inhomogeneous distribution and orientation of the fibers in injection molded GFP parts, which causes the material to become birefringent. In order to test the mechanical strength of the sample non-destructively, the birefringence and orientation of the optical axis in the sample can be detected by PS THz measurements [6]. Apart from the large penetration depth of THz waves, time-domain (TD) THz systems exhibit several beneficial characteristics:

First of all, the THz pulse necessarily contains a bandwidth of wavelengths. Instead of dis-

#172500 - $15.00 USD Received 12 Jul 2012; revised 12 Sep 2012; accepted 13 Sep 2012; published 24 Sep 2012

carding most of this spectral information [7], it may be used in, e.g., THz ellipsometry [8] to determine the (anisotropic) dielectric properties of a sample [9].

The second advantage is that electro-optic sampling and photo-conductive switches are coherent detection methods, i.e., the THz electric field is recorded [10], in contrast to "ordinary" optics where the power (spectrum) is measured. Therefore, by measuring the amplitudes and phases of both components of the electric field with a PS photo-conductive antenna (PCA) [11], the electromagnetic field is uniquely defined and no analyzer is needed [12]. Instead of using a wire grid filter as analyzer or a second detector, we realized the PS detector by a three-contact PCA similar to the one used in [13] but did not take orthogonal detection axes for granted [14]. Not surprisingly retaining the phase information of the complex signals proves to be crucial for the retrieval of birefringence. Interestingly to note, in [15] both components of the THz pulse were measured by using a circularly polarized probe beam, but only the relative difference of the signal amplitudes was evaluated.

Additionally to the bandwidth of the THz pulse and a PS detection method we exploit an approach inherited from PS optical coherence tomography [16] where a quarter-wave plate is used to convert linearly polarized light to circular polarization. While linearly polarized light can be favorable for certain samples, e.g. for defect detection on surfaces of carbon fiber composites [17], for birefringence measurements it means that the polarization direction has to be rotated with regard to the sample. If the polarization axis of the THz beam coincided with either the fast or slow optical axis of the sample, only a single phase shift of the pulse would be observed, but no information on the second axis or the birefringence of the material could be obtained. Hence, at least a second measurement with a rotated polarization axis or sample is necessary to compensate for this ambiguity, but rotating the polarizer can also introduce shifts in the relative phases of the signals [10]. Alternatively, one can rotate the sample [18, 19], which is only practicable if it is homogenous. However, a circularly polarized light does not suffer from this degeneracy and both the slow and the fast optical axis in the sample contribute to the measurement signals. Hence, rotations of the THz pulse or the sample are avoided; moreover, no polarization filter is needed at all. We use a Fresnel prism made of high-resistive silicon [20] to introduce a phase shift of $\frac{\pi}{2}$ between horizontal and vertical field components, i.e., the initially linearly polarized THz pulse becomes circularly polarized.

All together these ingredients allow us to determine the birefringence and orientation of the optical axis in a single measurement without having to rotate the polarization axis of the THz beam with regard to the sample. Furthermore, the presented analysis algorithm neither relies on orthogonal detection axes nor on reference measurements of the initial THz pulse. This special arrangement of the setup also calls for a thorough analysis of the acquired data. We found remarkably simple equations that connect the Fourier components of the signals with the birefringence and orientation of the optical axis in the material. Above all, if the PCA is positioned to give identical pulse shapes on both arms, the detection axes do not need to be orthogonal and no knowledge about the initial phase relations of the pulse is needed. This property simplifies adjustment and increases the stability of the measurement setup.

2. Materials & methods

2.1. Experimental setup

The used setup is a modification of our recently developed scanning THz imaging system, which is described in detail in [1]. Generation and detection of the THz pulse is realized by PCAs made of low-temperature grown gallium arsenide (LT-GaAs) and a femtosecond laser (pulse length $< 100\,\mathrm{fs}$) operating at $790\,\mathrm{nm}$. Lateral imaging is performed by two mirrors mounted on a two-axes galvano scanner and with a scanning lens made of polytetrafluoroethylene, which focuses the THz beam on the sample with a diffraction limited spot size of about

#172500 - $15.00 USD Received 12 Jul 2012; revised 12 Sep 2012; accepted 13 Sep 2012; published 24 Sep 2012

3 mm in diameter. A retroreflector mounted on a mechanical linear translation stage forms the temporal scan axis. After the sample has been mounted in a holder no further movements are necessary for the three-dimensional scan, which is performed as consecutive en-face scans, i.e., the lateral scan represents the fast scan directions, whereas the depth scan forms the slowest axis.

For this work two changes have been made to the setup, which is shown in Fig. 1. First, a Fresnel prism made of high resistive silicon is inserted between the THz beam splitter and the galvano scanner. The base of the prism comprises an isosceles triangle with an apex angle of 96°. If the THz beam enters the front faces at a right angle, the angle of incidence on the back side of the prism is 42°, which will lead to total reflection occuring at this face. For this angle of incidence and together with the refractive index of $n = 3.416$ for silicon in the THz range, the introduced relative phase shift between the horizontal and vertical components of the THz field is $\frac{\pi}{2}$ [2]. This phase shift occurs twice, once before the sample is illuminated and also after the reflection by the sample. Thus, in case of an isotropic material, the polarization axis of the detected THz beam is rotated by 90° with regard to the emitted beam [21]. The polarization direction is set to $-45°$ by the polarizer in front of the beam splitter, which is then rotated to $+45°$ after passing the Fresnel prism twice when a metallic mirror is used as the sample.

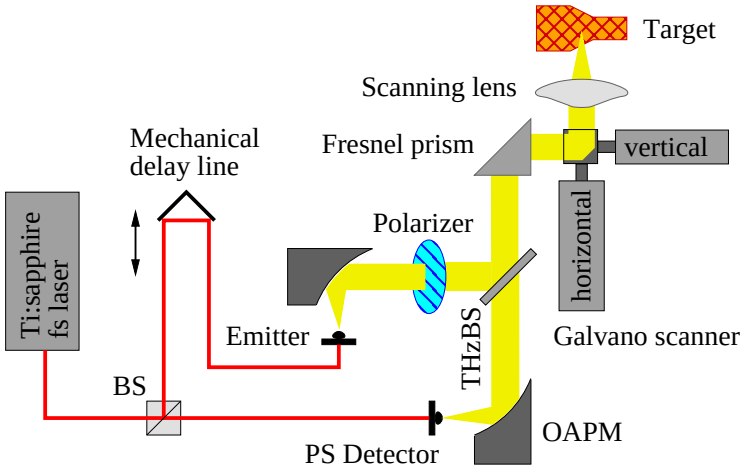

Fig. 1. Schematic drawing of the measurement setup. BS = non-polarizing infrared beam splitter, OAPM = off-axis parabolic mirror, THzBS = THz beam splitter. The light path of the infrared beam is drawn in red and that of the THz pulse in yellow.

The second modification affects the detector. The dipole detector from [1] is replaced by the PS PCA shown in Fig. 2. The diagonal electrode forms the common ground for the horizontal and vertical gaps, which have a width of 10 µm and a distance of 5 µm. The signals of both arms are amplified (DLPCA-200 from Femto) and fed into the two inputs of a single lock-in amplifier (eLocke203 from Anfatec). Thus, it is possible to detect both signals in one measurement, which are ultimately recorded by a DAQ card (6281 from National Instruments) and a personal computer, which also controls the linear translation stage and the galvano scanner.

One problem arises from the fact that a current may also flow directly between the horizontal and vertical electrode [14]. Among other things this crosstalk depends on the exact location of the spot of the probe beam on the antenna. In fact, it is almost impossible to get rid of it completely, which results in non-orthogonal effective detection axes indicated by the black solid and dashed lines in Fig. 2. In order to find the orientation of the detection axes, a polarization filter is put in front of the detector and rotated between 0° (horizontal) and 90° (vertical). Both

#172500 - $15.00 USD Received 12 Jul 2012; revised 12 Sep 2012; accepted 13 Sep 2012; published 24 Sep 2012

a horizontal and a vertical orientation of the analyzer result in non-vanishing signals on both channels of the lock-in amplifier. The ratio of the amplitude of the THz pulse at vertical and horizontal orientation gives the tangent of the angle α between detection and the horizontal axis (see Fig. 2). We found that this angle can only be minimized by adjusting but never vanishes completely.

For alignment of the PS antenna we use a mirror as the target and not only maximize the sum of the amplitudes of the two components of the THz pulse, but also minimize the area between the two pulses. For this purpose, the outputs $s_a(t)$ and $s_b(t)$ of both channels of the lock-in amplifier are recorded during a depth scan and the area $\int |s_a(t) - s_b(t)|$ is calculated. Minimizing this figure of merit guarantees that both the signal amplitudes and shapes of the two measured components are identical. Once this inital setup of the system has been finished, the sample, in our case an injection molded GFP part, can be inserted. In Fig. 3(a) the left pulse stems from the reflection on the front side of the sample. It can be seen that both the inital amplitude and waveform of both signals still match. At a time delay of 55 ps the reflection from the back side of the sample is visible. Due to birefringence in the material the components along the fast and slow axis experience different phase shifts and hence the pulses become distorted. The main task of this work will be to recover the birefringence and optical axis from these two signals. We will restrict ourselves to the case of a free standing optically thick sample, i.e., the reflections from the front and back side can be clearly separated.

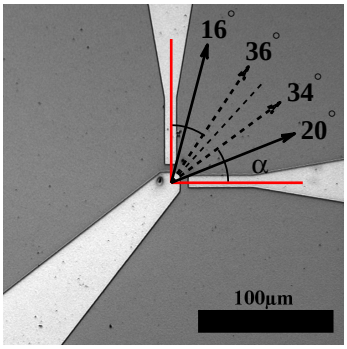

Fig. 2. Photomicrograph of the electrode structure on the polarization sensitive antenna. The diagonal electrode acts as the common ground for the horizontal and vertical gaps. Depending on the positioning of the laser spot the detection axes (black solid and dashed lines) are tilted with regard to the horizontal and vertical axes (indicated by red lines). The thin dashed line indicates the polarization direction of the THz beam along the 45° diagonal.

In Fig. 3(b) we present the dynamic range of the system. It is obtained by Fourier transformation of the pulse reflected by a mirror and normalized by the respective noise levels of the two channels. The maximum dynamic range is 370 at a frequency of 230 GHz for a lock-in time constant of 5 ms. The usable bandwidth is limited up to 1.5 THz, which is roughly 75% of the bandwidth available with a dipole detector. A noticeable difference between the spectra of the two detector arms is visible above 1 THz. Because also the noise levels of both detection arms differ, we suspect inhomogeneities of the PCA substrate or differences in the electrical pathways of the two signals to be the cause. Differences in the wire bondings of the electrode structures can have an influence on the eigenmodes of the antenna, and the two pre-amplifiers are also unlikely to be identical. Due to the lithographic fabrication process, geometric differences of the electrode structures are not expected to be the reason for the discrepancy between

#172500 - $15.00 USD Received 12 Jul 2012; revised 12 Sep 2012; accepted 13 Sep 2012; published 24 Sep 2012

the two spectra. Anyway, we will limit our analysis to frequencies smaller than 1 THz. It is noted that for sample measurements the usable bandwidth can become smaller than the specified value, as it is also influenced by the absorption of the investigated material.

As described above, upon adjustment of the probe beam a wire grid polarizer is put in front of the detector to determine the orientation of the detection axes. For the given alignment we find that the vertical gap detects the THz field along an axis inclined at 16° to the vertical, whereas the main direction of the horizontal gap is turned out of the horizontal by 20°. For the analysis of the signals a mean value of 18° will be used, and a symmetry with regard to the 45° polarization direction will be assumed. Thus, two crucial requirements for an easy data analysis are met. First, the amplitudes of the Fourier components of both signals are equal. Second and most importantly, the same pulse shape also ensures identical initial phases of the Fourier components for both signals, as will be shown to be indispensable by the analysis below.

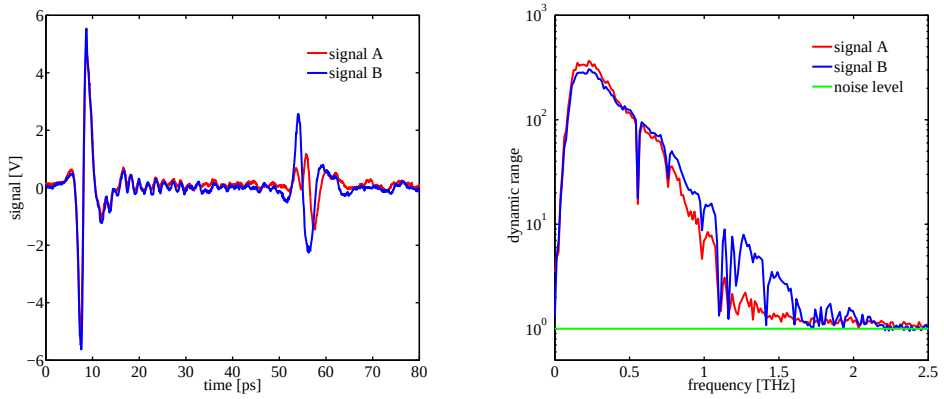

(a) (b)

Fig. 3. (a) Time domain signal of the two channels of the PS detector during a depth scan of a birefringent sample. Birefringence in the sample distorts the second pulse reflected from the backside. (b) Dynamic range of the two channels calculated by Fourier transformation of the signals reflected from a mirror and scaled by their respective noise levels.

2.2. *Parameter extraction*

The material parameters are calculated in the spectral domain. We start our mathematical with a description of the system with Jones matrices:

$$\begin{pmatrix} S_a \\ S_b \end{pmatrix} = S(f)e^{\imath\varphi_0(f)} \begin{pmatrix} 1 & \varepsilon \\ \varepsilon & 1 \end{pmatrix} \cdot F \cdot R(-\theta) \cdot \begin{pmatrix} e^{\imath\varphi_1} & 0 \\ 0 & e^{\imath\varphi_2} \end{pmatrix} \cdot R(\theta) \cdot F \cdot \begin{pmatrix} 1 \\ -1 \end{pmatrix}. \quad (1)$$

The initial THz pulse depicted by the last term is linearly polarized at $-45°$. The amplitude spectrum $S(f)$ and the pulse form, represented by a common phase factor $\exp(\imath\varphi_0)$ for horizontal and vertical components, will disappear in the final equations, since only normalized absolute values will be used. The action of the Fresnel prism is described by $F = \begin{pmatrix} 1 & 0 \\ 0 & \imath \end{pmatrix}$, which is passed twice by the THz beam. The orientation of the slow axis (larger refractive index) of the sample is at an angle θ with regard to the horizontal axis and enters the equation through the rotation matrices R. φ_1 and φ_2 are the phase shifts induced by the slow and fast

#172500 - $15.00 USD Received 12 Jul 2012; revised 12 Sep 2012; accepted 13 Sep 2012; published 24 Sep 2012

optical axes of the sample, respectively. Finally the non-orthogonal but symmetric detector is described by the parameter $\varepsilon = \tan\alpha$, where α is the angle between detection and horizontal or vertical axis as shown in Fig. 2, respectively. S_a and S_b are the complex frequency dependent spectral components of the two signals, obtained by Fourier transformation of the detected pulse that originates from the sample/air interface at the back. The pulse arising from the front surface is discarded, or even better, not recorded at all to save measurement time. Note, that for each frequency component the vector describing the initial polarization is normalized to $\sqrt{2}$. After a short computation and with $\tilde{S} = S(f)\exp(\imath\varphi_0)$ one finds

$$S_a + S_b \quad = \quad \tilde{S}(1+\varepsilon)\left(e^{\imath\varphi_1} + e^{\imath\varphi_2}\right) . \tag{2}$$

This equation is remarkable as it is independent of the angle θ. We make an ansatz for the phase shift $\Delta\varphi$ induced by the birefringent material, thereby neglecting any dispersion:

$$\varphi_j = \varphi_0 \pm \frac{\Delta\varphi}{2} = \varphi_0 \pm \frac{2\pi}{c_0} d\Delta n f \quad , \tag{3}$$

$j = 1$ for upper and $j = 2$ for lower sign, respectively. The optical path length $2dn$ is twice the geometrical thickness of the sample times the refractive index. The birefringence of the material is Δn and f the frequency. With a definition for the spectral energy

$$A^2 \quad := \quad \frac{|S_a|^2 + |S_b|^2}{2} = |\tilde{S}|^2\left(\varepsilon^2 + 2\varepsilon\cos\Delta\varphi + 1\right) \tag{4}$$

and using Eq. (2) we obtain

$$\frac{|S_a + S_b|}{\sqrt{\left(|S_a|^2 + |S_b|^2\right)/2}} \quad = \quad \frac{|S_a + S_b|}{A} = \frac{2\,(1+\varepsilon)\left|\cos\frac{\Delta\varphi}{2}\right|}{\sqrt{\varepsilon^2 + 2\,\varepsilon\,\cos\Delta\varphi + 1}} . \tag{5}$$

An obvious requirement for stability restricts the detection axes to non-degenerate cases $0 \le \varepsilon < 1 \Rightarrow 0 \le \alpha < 45^\circ$.

The first minimum of Eq. (5) at frequency f_{min} lets us calculate the birefringence

$$\Delta\varphi(f_{min}) = \pi \Rightarrow \Delta n = \frac{c_0}{4 f_{min} d} . \tag{6}$$

The detectable birefringence is therefore restricted by the available bandwidth of the THz pulse and the sample thickness, viz. $\frac{c_0}{4\Delta n d} <$ bandwidth. For a 4 mm thick sample and a bandwidth of 1 THz the minimum birefringence is therefore about 0.02.

In order to extract the orientation θ of the optical axis we form the equation

$$\frac{|S_a|^2 - |S_b|^2}{|S_a|^2 + |S_b|^2} = \frac{|S_a|^2 - |S_b|^2}{2A^2} \quad = \quad \frac{(1-\varepsilon^2)\sin(\Delta\varphi)}{\varepsilon^2 + 2\varepsilon\cos(\Delta\varphi) + 1} \cdot \sin(2\theta) . \tag{7}$$

When seen as a function of $\Delta\varphi(f)$, this is a distorted sine wave with an amplitude $\sin 2\theta$. A closer analysis shows that this amplitude is independent of the parameter ε (see Fig. 5(b)). This amplitude therefore permits to determine the orientation of the slow optical axis with respect to the horizontal.

3. Results & discussion

The developed algorithm is tested for an injection molded GRP sample showing birefringence at THz frequencies. In Fig. 4(a) a photograph of the sample with a thickness of 4 mm is shown.

#172500 - $15.00 USD Received 12 Jul 2012; revised 12 Sep 2012; accepted 13 Sep 2012; published 24 Sep 2012

The material is high density polyethylene (HDPE) reinforced with 50 % glass fibers by weight. An equivalent sample was also used in [6] for transmission measurements, where the fiber orientation in a single point was extracted with three different orientations of the sample. Figure 4(b) is obtained by integrating the spectral energy density (see Eq. (4)) of the reflected THz pulse for frequencies between roughly 0.1 and 1 THz.

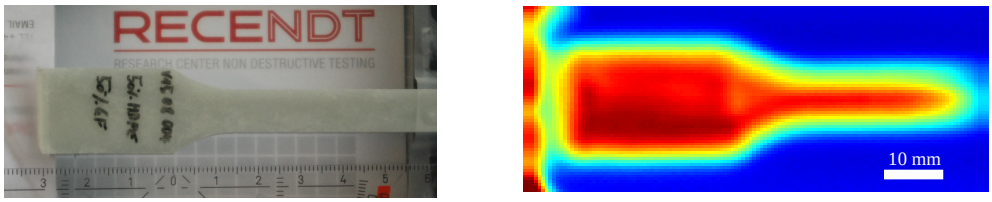

(a) (b)

Fig. 4. (a) Photograph of the injection molded GFP part. (b) Reflectance of the sample in the THz range (see text).

In order to extract the birefringence Δn, the first minimum of the normalized linear combination $|S_a + S_b|$ is searched (see Eq. (5)). For illustration, we show the frequency dependence of this superposition in a single point in Fig. 5(a). The black solid line is calculated from the measured data, and the dashed line is the theoretical behaviour of an ideal detector ($\varepsilon = 0$). The theoretical prediction for a detector with $\varepsilon = \tan 18^\circ$ is shown in red. The accuracy of the frequency minimum f_{min} is determined by the spectral resolution of the measurement. If all points with a minimum larger than a threshold value of one are rejected, this procedure is remarkably stable. The frequencies found are illustrated in Fig. 5(c), where the rejected pixels are drawn in blue. From these minima the birefringence can be calculated with Eq. (6); the resulting values give the color coding in Fig. 6.

Determination of the optical axis θ requires a more careful approach. Starting at f_{min}, the local extrema of $(|S_a|^2 - |S_b|^2)$ occurring to the left and right of this frequency are searched (see Eq. (7)). Again the measurement data is drawn as the black solid line in Fig. 5(b). For an ideal detector, a simple sinusoidal behaviour is expected, indicated by the dashed line. However, good agreement can be found when the parameter $\varepsilon = \tan 18^\circ$ is used again, at least for frequencies smaller than the extremum to the right of f_{min}, as can be seen by the red line. It should be emphasized that the amplitude of this oscillation is solely determined by the orientation of the optical axis, irrespective how large the non-orthogonality of the detector is.

We note that the obtained curve is not centered on the abscissa, as would be expected from Eq. (7). One reason for this deviation is that the amplitudes of the two detection channels are only constant while scanning along the fast scan axis, where the scanning mirror forms a telecentric sytem with the scanning lens, and the THz beam stays parallel to the optical axis. When scanning along the slow lateral axis, the amplitudes of the signals drop to either side [1], but unfortunately with a small difference for the two signals. Also, the description of the detector with a single non-ideality factor ε is only an approximation, and actually the angles for the two detection axes are not exactly equal, as can be seen in Fig. 2. All these factors cause the minimum in Fig. 5(a) to be larger than zero and also create the offset of the curve in Fig. 5(b). Albeit these shortcomings complicate the numerical analysis, the obtained results agree well with former measurements in transmission [6].

Finally, the combined results of birefringence and direction of optical axis are presented in Fig. 6(a). The colors are given by the magnitude of the birefringence Δn, and the arrows indicate the orientation of the slow optical axis, which is expected to correspond to the preferred

#172500 - $15.00 USD Received 12 Jul 2012; revised 12 Sep 2012; accepted 13 Sep 2012; published 24 Sep 2012

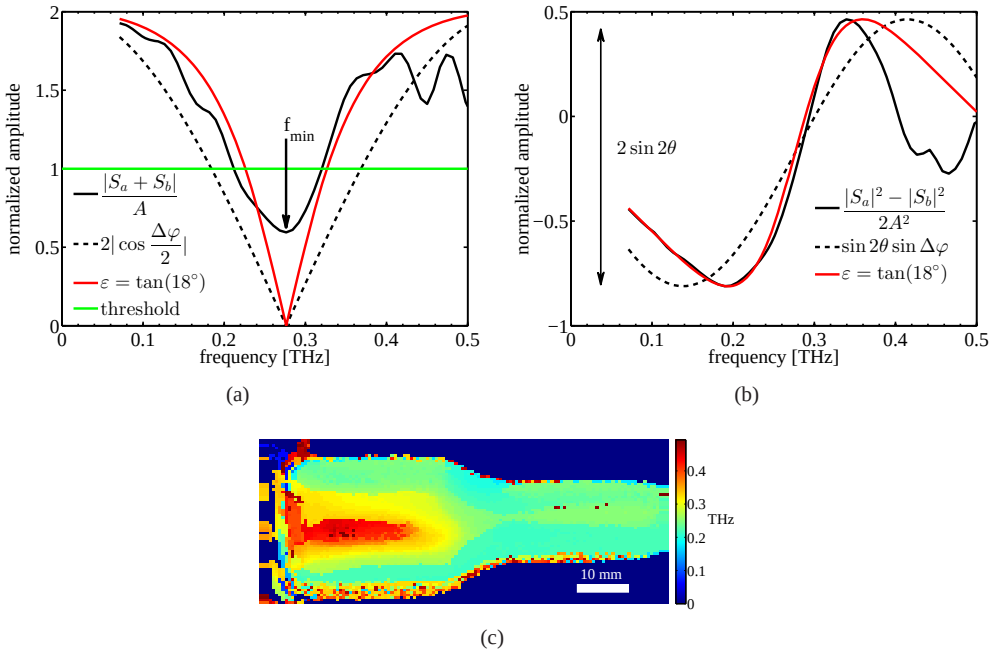

Fig. 5. (a) Determination of the minimum frequency f_{min} from Eq. (5) for calculating the birefringence. Points with a minimum larger than the threshold value of 1 are rejected. (b) Extraction of the amplitude in Eq. (7) for computation of the optical axis. (a) and (b) Black solid lines are measurement, the dashed line is the theoretical curve for an ideal detector ($\varepsilon = 0$), and solid red lines are calculated with $\varepsilon = \tan(18°)$. (c) Image of the extracted minimum frequency for the GRP sample.

alignment of the glass fibers averaged over the sample thickness. During injection molding the material was injected on the left hand side. From our results we infer a slightly asymmetric flow of the molten mass. The directed flow along the edges and the laminar flow through the parallel channel on the right hand side leads to a higher ordering of the glass fibers, which results in a higher birefringence compared to the region in the middle left. Maximum values of the birefringence of 0.1 are observed. Also the direction of the optical axis follows the contour of the neck of the sample. However, the analysis algorithm breaks down right at the edges of the sample, which we attribute to scattering and reflections from the side walls [15].

We have repeated the measurement with a much less ideal ($\varepsilon \approx \tan 35°$) but more symmetric detector adjustment. As can be seen in Fig. 2, the detection axes are nearly collinear, which indicates a less ideal adjustment of the laser spot with regard to the gaps and hence increased crosstalk. In addition, a higher scan resolution and a slightly different scan area were chosen. The result is shown in Fig. 6(b) and agrees well with our former measurement. This clearly confirms the stability of our measurement and parameter extraction algorithm.

4. Conclusion

We have presented an advanced setup for PS THz imaging and developed an algorithm for the extraction of birefringence and the orientation of the optical axis, which exhibit several advantages:

Measurements in reflection geometry automatically double the optical path length in the

#172500 - $15.00 USD Received 12 Jul 2012; revised 12 Sep 2012; accepted 13 Sep 2012; published 24 Sep 2012

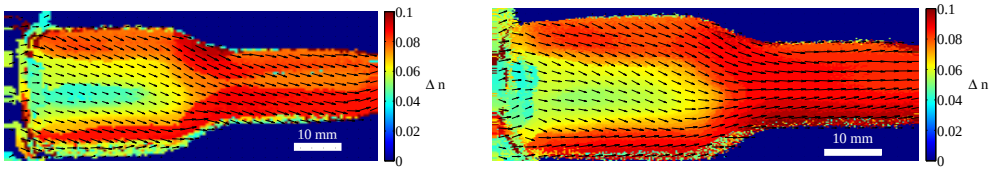

(a) (b)

Fig. 6. Birefringence (color coded) and orientation of the slow optical axis (black arrows). (a) is obtained with the detection axes tilted by about 18°. For (b) the detection axes were nearly collinear (tilt angle 35°) but more symmetric.

sample, thereby lowering the detectable birefringence by a factor of two. Furthermore, the usage of a quarter-wave plate means that a single measurement with a fixed polarizer orientation can be realized, and still an arbitrary orientation of the optical axis of the sample can be determined. It is impossible to achieve the same with a linearly polarized THz beam, where at least two measurements have to be performed with a rotation of the sample with respect to the direction of the polarization in order to break the ambiguity between orientation of the polarization and the optical axis. This can be avoided if the THz pulse is circularly polarized, meaning that the measurement time is not extended in comparison to a conventional setup. In [15] it was suggested to split the THz beam and use a second detector for recording both components simultaneously. If the PS PCA is properly adjusted, a single PS detector is sufficient and one can get around the losses of the beam splitter and polarizers. Finally, any errors induced by wire-grid analyzers are eliminated, which are usually used to detect the two components of the THz field [22].

Our analysis algorithm does not rely on a reference pulse, but calculates the birefringence and orientation of the optical axis orientation solely from the relative difference between the two signals of the PS detector. This method is therefore insensitive to drifts in the measurement setup, which affect both signals likewise and could, e.g., influence the pulse shape and phase relations of the frequency components of the THz pulse, which represents a common problem for rather long measurement times. It is also quite insensitive to the preferred direction of the detector, which is important because the detection axes are usually hard to control during adjustment. An optimal adjustment can be found when the sum of the detected THz pulse amplitudes is maximized, and at the same time the integrated difference of the pulse shapes is minimized. This should automatically give symmetric detector axes, as well as identical phase relations for the initial components of the THz pulse.

We have tested our approach for a GRP sample, where it was used to study the birefringence and orientation of the optical axis, induced by the integral orientation of glass fibers in the polymer. A high ordering of the fibers was assigned to high birefringence, whereas low birefringence was indicative for a turbulent flow of the melt during injection molding. These results clearly show the applicability of our developed method for the investigation of birefringent samples.

Using THz waves allows measuring thick samples of several millimeters to centimeters, which are otherwise opaque in visible or near infrared light. Therefore, PS THz imaging provides unprecedented potential for nondestructive mapping of anisotropies in materials, which can hopefully be exploited by advanced methods such as developed in this work.

#172500 - $15.00 USD Received 12 Jul 2012; revised 12 Sep 2012; accepted 13 Sep 2012; published 24 Sep 2012

Acknowledgments

This work has been supported by the Austrian Science Fund FWF (Project L507-N20), by the European Regional Development Fund (EFRE) in the framework of the EU-programme Regio 13, and the federal state of Upper Austria.

#172500 - $15.00 USD Received 12 Jul 2012; revised 12 Sep 2012; accepted 13 Sep 2012; published 24 Sep 2012